RSC Advances

Cite this: *RSC Advances*, 2011, **1**, 1822–1833

www.rsc.org/advances

PAPER

Phase behavior of mesoporous nanostructures templated by amphiphilic crystalline–crystalline diblock copolymers of poly (ethylene oxide-*b*-ε-caprolactone)†

Jheng-Guang Li and Shiao-Wei Kuo*

Received 24th June 2011, Accepted 31st August 2011
DOI: 10.1039/c1ra00349f

A crystalline–crystalline diblock copolymer, poly(ethylene oxide-*b*-ε-caprolactone) (PEO-*b*-PCL), was synthesized through ring-opening polymerization using monomethoxy-poly(ethylene oxide) as a macro-initiator. The amphiphilic double-crystalline diblock copolymer was used as a template to prepare highly-ordered mesoporous silicas and phenolic resins using an evaporation-induced self-assembly (EISA) method. The mesophase transformation of mesoporous nanostructures, which contained different tetraethyl orthosilicate (TEOS) and phenolic resin contents, was investigated using small-angle X-ray scattering (SAXS) and transmission electron microscopy (TEM) analyses. The SAXS profiles revealed a sharp primary peak and highly long-range order reflections such as a cylinder or gyroid structures, at certain compositions of TEOS and phenolic resins, which was consistent with the TEM images. Fourier transform infrared spectroscopy (FTIR) analyses provided positive evidence that the ether group of PEO is a stronger hydrogen bond acceptor than the carbonyl of PCL with the hydroxyl group of TEOS or phenolic resin, resulting in the excluded and confined PCL phase. This is the first report suggesting that differential scanning calorimeter (DSC) analysis could be utilized as a convenient method to differentiate the morphology of mesoporous nanostructures in a crystalline–crystalline diblock copolymer.

Introduction

Ordered mesoporous materials with a high surface area, large pore volume, and mechanical stability, have received much attention for their potential applications in adsorption, separation, catalysis, photonics, and drug delivery in recent years.[1–44] Mobil scientists first reported the synthesis of mesoporous silicas using cationic surfactants such as cetyltrimethylammonium bromide ($C_{16}H_{33}N(CH_3)_3Br$, CTAB) as the template to obtain highly-ordered mesoporous molecular sieves (M41S) under hydrothermal and basic conditions.[45,46] Following that report a large number of studies were conducted to investigate the formation of mesostructures on the basis of low molecular weight surfactants by cooperation of self-assembly or true liquid-crystal templating processes.[47–52] A dominant strategy involves templating of the mesophase growth by volatile solvent evaporating induction and is known as the evaporation-induced self-assembly (EISA) strategy. This technique is an alternative synthetic approach that allows the tuning of inorganic condensation with the formation of a *meso*-organized liquid-crystal template.[14,53–65] As the solvent is removed, a mesophase is gradually formed.

Amphiphilic block copolymers provide a versatile platform for fabricating large-area periodic nanostructures by controlling the self-assembly behavior, with length scales varying from a few nanometres to several hundred nanometres. Furthermore, block copolymers have attracted particular interest due to their ability to form a rich variety of self-assembling nanostructures, such as lamellar, hexagonally packed cylindrical, and body-centered cubic micellar structures as a result of the relative volume fractions of the blocks, total degree of polymerization, and Flory–Huggins interaction parameter; some examples include ref. 66–75.

However, the majority of amphiphilic diblock copolymers are water insoluble, and the EISA strategy becomes very important when fabricating various mesoporous nanostructures with large pores. A variety of synthetic strategies have been developed based on poly(ethylene oxide)-*b*-poly(propylene oxide)-*b*-poly (ethylene oxide) (PEO-PPO-PEO) triblock copolymers as templates to obtain many highly ordered large-pore mesoporous silicas.[58,62,64,76–96] Commercially available PEO-PPO-PEO triblock copolymers are seldom able to directly template ordered mesoporous silicas with pore sizes larger than 12 nm because of molecular weight and composition limitations. High-molecular-weight copolymers with long hydrophobic segments, such as poly(ethylene-oxide-*b*-styrene) (PEO-*b*-PS), are promising

Department of Materials and Optoelectronic Science, Center for Nanoscience and Nanotechnology, National Sun Yat-Sen University, Kaohsiung, 804, Taiwan. E-mail: kuosw@faculty.nsysu.edu.tw
† Electronic Supplementary Information (ESI) available. See DOI: 10.1039/c1ra00349f/

candidates to template large-pore mesoporous silicates because the pore dimensions are primarily related to the molecular weights of the hydrophobic segments.[55,61]

Similar to the inorganic–organic assembly for mesoporous silicas, the organic–organic self-assembly approach has also been successfully used to synthesize ordered mesoporous carbon frameworks.[54,57–59,97–104] Recently, a family of carbon mesostructures, including two-dimensional (2-D) hexagonal (space group of *p6mm*), 3-D bicontinuous ($Ia\bar{3}d$), body-centered cubic ($Im\bar{3}m$) and lamellar symmetries, was prepared using phenolic resins as a carbon source and PEO-PPO-PEO triblock copolymers as templates.[57–58,98–99] The pore sizes of mesoporous carbons were limited due to the low molecular weight copolymers. Employing ordered mesoporous silica such as SBA-15[76,77] and KIT-6[105] as hard templates can replicate carbon with an ordered mesostructure and large porosity; this result was thought to be a breakthrough in the area of mesostructured materials.[106–108] A new synthetic strategy for the preparation of ordered mesoporous carbons with diverse mesostructures has been developed based on the organic–organic self-assembly between PEO-PPO-PEO templates and thermosetting phenolic resin precursors for the direct templating-synthesis of ordered mesoporous carbons with various pore structures. Here, a lab-made diblock copolymer PEO-*b*-PCL (M_w = 14 600) was synthesized as a new template to prepare ordered mesoporous carbons using an EISA strategy. The pore size of ordered mesoporous carbons was 11 nm in the presented study.

The PEO-*b*-PCL diblock copolymer consisted of two immiscible crystallizable blocks wherein both PEO and PCL blocks could form hydrogen bonds with the phenolic resin. In the A-*b*-B/C diblock copolymer/homopolymer blends, microphase separation occurred from the disparity in the intermolecular interactions.[70–75,109–112] The hydrogen bonding between PEO and the phenolic resin was significantly stronger than that between PCL and the phenolic resin. Selective hydrogen bonding between the phenolic/PEO pair at relatively lower phenolic contents and co-existence of two competitive hydrogen bonding interactions between phenolic/PEO and phenolic/PCL pairs at relative higher phenolic contents were observed in this blend.[113] This effect leads to the formation of a variety of composition-dependent nanostructures, including disordered, gyroid and short cylinder. Similar to the silica/PEO-*b*-PCL films, as the ratios of the TEOS/PEO-*b*-PCL mixtures increase, the morphologies of the mesophase change from a long cylinder to a short cylinder. To the best of our knowledge, no studies have been reported on making use of the self-assembly of double crystalline PCL-based amphiphilic diblock copolymers as structure-directing agents in the synthesis of mesostructured silica and phenolic resin films. As a result of the special confinement effect of the double crystalline amphiphilic PEO-*b*-PCL diblock copolymer, we can utilize a convenient method that uses DSC to characterize the morphology of mesoporous nanostructures in a crystalline–crystalline diblock copolymer PEO-*b*-PCL, but it does not work in a crystalline–amorphous diblock copolymer such as PEO-*b*-PS.[114] The phase behaviors and compete interactions of the mesostructures were investigated using Fourier transform infrared (FTIR) spectroscopy, high-resolution scanning electron microscopy (HRSEM), small-angle X-ray scattering (SAXS) and transmission electron microscopy (TEM) analyses.

Experimental

Materials

Monomethoxy-poly(ethylene glycol) with a molecular weight of 5000 (MPEG-5 K) was obtained from Fluka and dried by azeotropic distillation with dry toluene. ε-Caprolactone (ε-CL, Acros) was purified by vacuum distillation over CaH_2. The distillation fraction collected at 96–98 °C (5 mm-Hg) was used in all polymerization. Stannous(II) octoate [$Sn(Oct)_2$, Sigma Corp.] was used as received. Methylene chloride was dried over CaH_2 prior to use. The phenolic was synthesized with sulfuric acid in a condensation reaction, which produced average molecular weights (Mn = 500) that are described in previous studies.[115–118] Hexane, tetrahydrofuran (THF), tetraethyl orthosilicate (TEOS), HCl, and HMTA (all from Aldrich) were used as received. Deionized water was used for all experiments.

Synthesis of PEO-*b*-PCL block copolymer[119]. Block copolymers were readily prepared through the ring-opening polymerization of ε-CL and mPEG5000 in the presence of stannous octoate as the catalyst. The reaction mixtures were prepared by introducing, a desired volume of ε-caprolactone monomer into a silanized flask containing a pre-weighed amount of mPEG5000 under a nitrogen atmosphere. One drop of $Sn(Oct)_2$ was added and the flask was connected to a vacuum line, evacuated, sealed off and heated to 130 °C. After 24 h, the resulting block copolymers were dissolved in methylene chloride and precipitated in excess of cold n-hexane. The polymers were dried at 40 °C under vacuum. (Yield: 72%), ^{1}H NMR (500 MHz, $CDCl_3$, Fig. S1†) : δ 4.10 (t, –O–CH_2–, PCL), 3.65 (s, –CH_2CH_2O–, PEO), δ 3.35 (s, –OCH_3, PEO), δ 2.30 (t, 2H, PCL), δ 1.63 (m, 4H, PCL), δ 1.38 (m, 2H, PCL); IR : 3350 cm^{-1} (self-associated hydroxyl group absorption of phenolic resin), 3525 cm^{-1} (free hydroxyl groups of phenolic resin), 3250 cm^{-1} (hydrogen-bonded hydroxyl with the ether group of PEO), 1734 cm^{-1} (amorphous carbonyl group of PCL), 1724 cm^{-1} (crystalline carbonyl group of PCL), 1705 cm^{-1} (hydrogen-bonded carbonyl group of PCL).

Synthesis of the mesoporous silicas[55]. Mesoporous silica was prepared using an EISA strategy in THF with the PEO-*b*-PCL diblock copolymer as a template and TEOS as the silica precursor. Prior to the subsequent direct calcination, a hydrothermal treatment was adopted. In a typical synthetic procedure, 0.1 g of TEOS and 0.10 g of 0.1 M HCl solution were added to 5 g of a THF solution of PEO-*b*-PCL diblock copolymer (approximately 2.0 wt%) with stirring for 30 min to form a homogeneous solution. The solution was poured into Petri dishes to evaporate the THF at room temperature for 48 h. The transparent films were collected and ground into powders. The powders were transferred into a PFA bottle containing 30 mL of a HCl solution (1.0 M) and hydrothermally heated at 100 °C for 3 days. The product was washed with water and ethanol, dried at room temperature, and calcined in air at 600 °C to produce white mesoporous silicas; the above calcinations were conducted in a furnace with a heating rate of 1 °C min^{-1} as shown in Scheme 1(a).

Synthesis of mesoporous phenolic resins[55,59]. Phenolic resin, HMTA, and PEO-*b*-PCL were dissolved in THF until the solutions were homogenous. THF was slowly evaporated at room

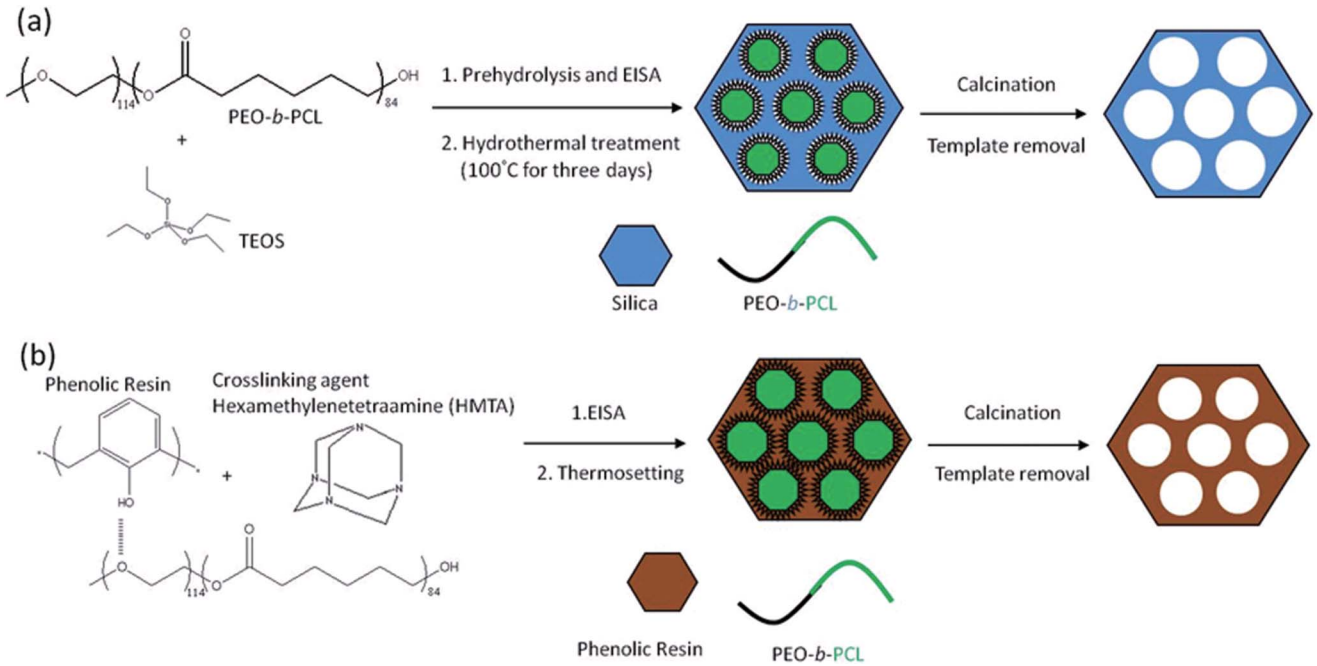

Scheme 1 Preparation of (a) mesoporous silicas and (b) mesoporous phenolic resins.

temperature, and the samples were subsequently vacuum dried at 30 °C for one day. Curing of the samples was performed using the following temperature profile: 100 °C for 2 h, 150 °C for 2 h, and 190 °C for 2 h. Pyrolysis of the crosslinked samples was performed by slowly heating from room temperature to 330 °C at a heating rate of 1 °C min^{-1} without a protective gas atmosphere.

Characterization. ^1H spectra were recorded at room temperature on a Bruker AM 500 (500 MHz) spectrometer using the residual proton resonance of the deuterated solvent as the internal standard and $CDCl_3$ as the solvent. Molecular weights and molecular weight distributions were determined by gel permeation chromatography (GPC) using a Waters 510 HPLC equipped with a 410 Differential Refractometer and three Ultrastyragel columns (100, 500, and 10^3 Å) connected in series; DMF was the eluent at a flow rate of 1.0 mL min^{-1}. Thermal analysis was performed using a Q-20 differential scanning calorimeter (DSC) from TA instrument. The measurement was operated at a heating rate of 20 °C and a cooling rate of 5 °C min^{-1} from 150 °C to −90 °C in N_2; the sample weighted between 5 and 10 mg. The thermal stability of the samples was characterized by using a TA Q-50 Thermogravimetric Analyzer operating under a nitrogen or a air atmosphere. The sample (approximately 7 mg) was placed in a Pt cell, and heated at a rate of 20 °C min^{-1} from 30 to 800 °C in a nitrogen flow rate of 60 mL min^{-1} or 1.4 °C min^{-1} to 330 °C, and Isothermal for 180 min in a air flow rate of 60 mL min^{-1}. FTIR spectra of the samples were recorded using the conventional KBr disk method. The spectra were recorded using a Bruker Tensor 27 FTIR spectrophotometer. SAXS measurements were taken on a Nanostar U small-angle X-ray scattering system (Bruker, Germany) using Cu Kα radiation (40 kV, 35 mA). The *d*-spacing values were calculated using the formula $d = 2\pi/q$. Nitrogen sorption isotherms were measured at 77 K with an ASAP 2020 analyzer. Prior to taking the measurements, the samples were degassed under vacuum at 200 °C for at least 6 h. The Brunauer–Emmett–Teller (BET) method was utilized to calculate the specific surface areas. Using the Broekoff–de Boer (BdB) sphere model, the pore volumes and pore size distributions were derived from the adsorption branches of isotherms, and the total pore volumes were estimated from the adsorbed amount at relative pressure (P/P_0 of 0.995). The calibration curve was obtained by using Silica–Alumina (part no. 004-16821-00) as a reference material and nitrogen as an adsorption gas. TEM experiments were conducted on a JEOL 3010 microscope (Japan) operated at 200 kV. High-resolution scanning electron microscopy (HRSEM) images were taken using a field emission JEOL JSM-6700F (Japan) operated at 30 kV.

Results and discussion

Synthesis of PEO-*b*-PCL

The PEO-*b*-PCL diblock copolymer with a high molecular weight (~14 600 g mol^{-1}) was easily prepared from a simple one-step ring opening polymerization (ROP) method. The number average molecular weights (M_n) of the prepared copolymers were determined from ^1H NMR spectra by comparing the peak intensity of MPEG-5 K (–CH_2CH_2O–, δ = 3.65 ppm) to that of PCL (–O–CH_2–, δ = 4.10 ppm), considering the molecular weight (M_n = 5000) for MPEG-5 K (Fig. S1, ESI†). Gel-permeation chromatography (GPC) reported a polydispersity index (PDI) of 1.48 for the PEO-*b*-PCL diblock copolymer. The TGA of PEO-*b*-PCL showed a weight loss of approximately 98 wt% in the temperature range from 320 to 430 °C under nitrogen (Fig. S2, ESI†), and it showed 94 wt% loss between 275 and 330 °C under air (Fig. S3, ESI†). This result implies that the template can be easily removed by pyrolysis both in nitrogen and air.

Phase behavior of mesoporous silicas

PEO-*b*-PCL is insoluble in water and ethanol because of the high molecular weight PCL segment. Therefore, the EISA approach in THF was employed to synthesize mesoporous silicas, phenolic resins, and carbon. DSC experiments were performed to investigate the thermal properties of the silica/PEO-*b*-PCL nanocomposites. Fig. 1 shows the DSC traces of pure PEO-*b*-PCL and silica/PEO-*b*-PCL nanocomposites recorded by the cooling scan at a cooling rate of 5 °C min^{-1}. The peak temperature of the crystallization exotherm is defined as the freezing temperature (T_f), at which a higher T_f corresponds to a faster crystallization rate. Previous works have reported that the T_f associates with the nonisothermal crystallization under a fixed cooling rate and displays a distinct correlation with the microdomain structure.[114,120–124] The pure PEO-*b*-PCL block copolymer exhibited a crystallization peak at 36 °C (PEO block) and 29 °C (PCL block).[112] The crystallization ability of the PEO block is restricted by the PCL block, which is covalently coupled to the other end of the PEO block. These results indicate that there are two separated crystalline microdomains in these diblock copolymers that are comprised of the PEO and PCL blocks. When the silica/PEO-*b*-PCL ratio was= 1/1, two crystallization behaviors (two exotherms) were found at 31 °C and −49 °C. The higher freezing temperature may be from the crystallization of the PEO block. The second exotherm found at a lower freezing temperature, which was not present in either the PEO or the PCL homopolymer, appeared with more supercooling. Chen *et al.*[114,120] reported that the degree of supercooling ($\Delta T = T_m^0 - T_f$, T_m^0 = 75 °C)[123] required to initiate crystallization in the lamellar microdomains (ΔT = 50 °C) is comparable to that associated with the PCL homopolymer (ΔT = 42 °C); exceedingly large undercoolings are required for crystallizations in the cylindrical microdomains (T_f = −50 °C,ΔT = 125 °C).[123] As a result, the second exotherm at a lower T_f (−49 °C) may be from the PCL block in a 2D cylindrical confinement (ΔT = 124 °C) because the lowest T_f of the PEO block in 3D sphere confinement was at −30 °C.[114] The crystallization kinetics exhibited distinct transitions at the compositions corresponding to the morphological transformation, which demonstrates the feasibility of exploiting the microdomain pattern by manipulating the crystallization kinetics of the block chains. When the ratio of silica/PEO-*b*-PCL was further increased to 5/1, the T_f of PCL rose slightly to −44 °C, and the T_f of PEO completely disappeared. This result was attributed to the mesophase transformation of the silica/PEO-*b*-PCL nanocomposite from a long cylinder to a short cylinder (determined by SAXS and TEM) and the crystal structure destruction of PEO domain. Further increasing the silica/PEO-*b*-PCL ratio to 10/1 yielded a very small T_f for PCL at approximately −49 °C from distorted short cylinders (determined by SAXS and TEM). In addition, when the silica/PEO-*b*-PCL ratio was increased to 15/1, both crystallization peaks disappeared, implying that the crystalline structures of both PEO and PCL blocks were destroyed.

The structures of mesoporous silicas templated by double crystalline amphiphilic PEO-*b*-PCL were first investigated using TEM and SAXS as shown in Fig. 2 and 3. The SAXS pattern in Fig. 2 for TEOS/PEO-*b*-PCL = 1/1 (named silica-*a*) shows the maximum intensity at approximately q^* = 0.267 nm^{-1} (d = 23.5 nm), and higher-order reflections at $3^{1/2}q^*$ and $2q^*$ were observed. A long cylinder structure was observed in the TEM image in Fig. 3a. When TEOS/PEO-*b*-PCL = 5/1 (see Fig. 2, named silica-*b*), the maximum intensity appeared at approximately q^* = 0.26 nm^{-1} (d = 24.1 nm), and higher-order reflections at $3^{1/2}q^*$ and $2q^*$ were observed; these data were characteristic for a short cylindrical structure, which is further confirmed by TEM as shown in Fig. 3b. It was found that the TEOS/PEO-*b*-PCL weight fractions had an influence on the formation of the mesostructure. As the ratio of TEOS/PEO-*b*-PCL increased, the products experienced a remarkable mesophase transformation from a long cylinder to a short cylinder. A TEM image of silica-*b* clearly indicates a hexagonal pore structure, which confirms that silica-*b*

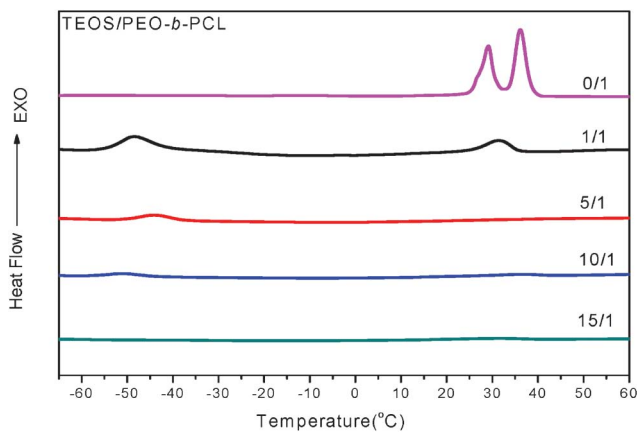

Fig. 1 DSC thermograms of the crystallization curve with different ratios of silica/PEO-*b*-PCL.

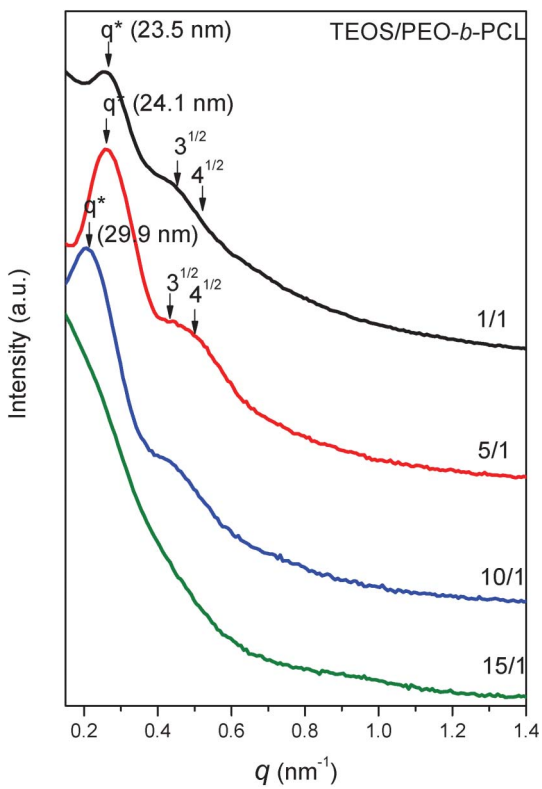

Fig. 2 SAXS patterns of mesoporous silicas templated by PEO-*b*-PCL with different TEOS/PEO-*b*-PCL weight fractions.

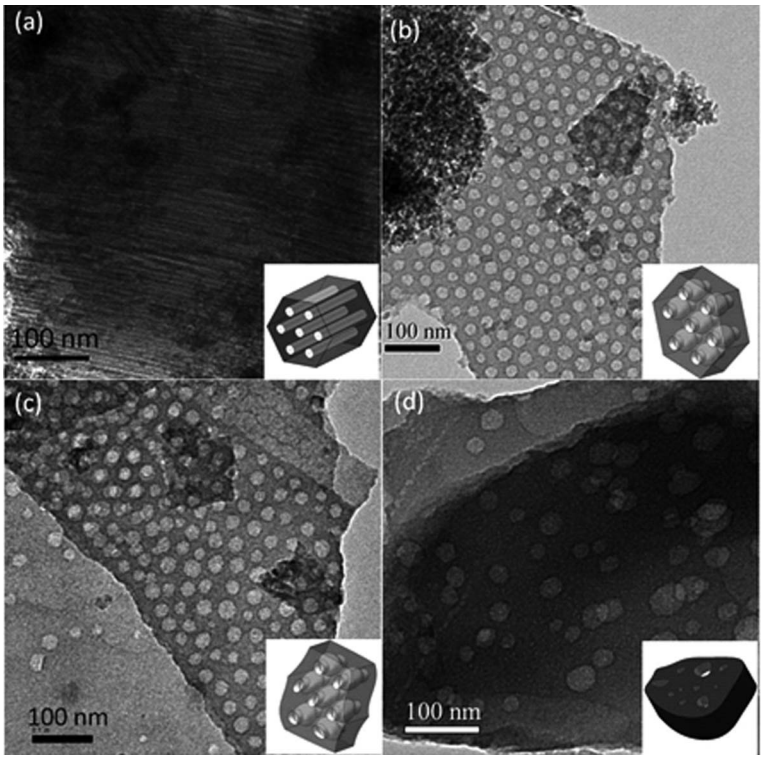

Fig. 3 TEM images of mesoporous silicas templated by PEO-*b*-PCL with different TEOS/PEO-*b*-PCL weight fractions: (a)1/1, (b)5/1, (c)10/1, and (d)15/1.

has a 2D hexagonal mesoporous structure. When the TEOS/PEO-*b*-PCL ratio increases, distorted short cylinders (silica-*c*, Fig. 2 and 3c) and disordered structures (silica-*d*, Fig. 2 and 3d) were observed because the ratio of the TEOS/PEO-*b*-PCL is too high to form long-range ordered structures. The TEM images provided additional evidence for the mesostructure changes. The transformation of mesoporous silicas from long cylinders to short cylinders was also in agreement with the FE-SEM measurements, as shown in Fig. 4. The FE-SEM image of silica-*a* in Fig. 4a displays a roughly flat surface and shows the side view of the hexagonal cylinder structure. However, the silica-*b* sample in Fig. 4b shows uniform and regularly aligned mesopores throughout the whole film, suggesting the top view of a highly ordered hexagonal cylinder mesostructure over a large domain. The morphological results were consistent with DSC analyses; the second exothermic peak (T_f = −49 °C) of TEOS/PEO-*b*-PCL = 1/1 was attributed to the mesophase for PCL crystallizations in a long cylinder of 2D confinement. The T_f raised slightly to T_f = −44 °C and corresponded to the mesophase transformation from a long cylinder to a short cylinder of TEOS/PEO-*b*-PCL = 5/1.

Nitrogen sorption isotherms of mesoporous silicas behaved like representative type IV curves with a sharp capillary condensation step in the relative pressure range of 0.85 to 0.95 as shown in Fig. 5A. This result indicates the generation of mesopores with an ultralarge uniform size. The silica-*a* sample exhibited an H_1-like hysteresis loop at P/P_0 = 0.4 to 0.9, which is indicative of a typical mesoporous structure with large cylindrical pores. The H_2 hysteresis loop found for silica-*b* was characteristic of the cage-like mesopores. On the basis of the Broekoff–de Boer (BdB) sphere model, the mean pore size measured from the adsorption branch was as large as 19.8 nm as shown in Fig. 5B. Similar isotherms with large H_2-type hysteresis loops can also be detected for silica-*c*. The mean pore size in Fig. 5B for silica-*c*, calculated from the BdB sphere model, was 22.5 nm and slightly larger than that of silica-*b*. The total pore volume and the total BET surface area of silica-*b* (0.33 $cm^3\ g^{-1}$ and 170 $m^2\ g^{-1}$, respectively), were smaller than those of silica-*a* (2.70 $cm^3\ g^{-1}$ and 1188 $m^2\ g^{-1}$, respectively, Table 1).These results confirmed the presence of the cage-like mesopores of short cylinders that were transferred from the cylindrical mesopores of the long cylinders. Because the PEO-*b*-PCL weight fraction of silica-*a* is much larger than that of silica-*b* and the block polymer part played the role of space in silica/PEO-*b*-PCL after calcinations, hence the BET surface area of silica-*a* is much larger than that of silica-*b*. Both silica-*c* and silica-*d* displayed H_2 hysteresis loops, implying a cage-like pore structure connected by small windows. The BET surface area, pore volume and BJH pore size of the silica materials are summarized in Table 1, indicating that the ratio of TEOS/PEO-*b*-PCL plays an important role in the determination of the described properties.

Phase behavior of mesoporous phenolic resins

Similar to the process with mesoporous silicas, we first investigated the thermal behavior of the phenolic/PEO-*b*-PCL blends using DSC. In general, DSC analysis is a convenient method used to determine miscibility and crystallization in polymer blends. Fig. 6 displays DSC thermograms for the phenolic/PEO-*b*-PCL blends (first cooling scan in Fig. 6b and second heating scan in Fig. 6a) and their curing products with HTMA at various constituent compositions (first cooling scan in Fig. 6c). The blends contain a block copolymer with two immiscible blocks, which is intended to exhibit two T_gs

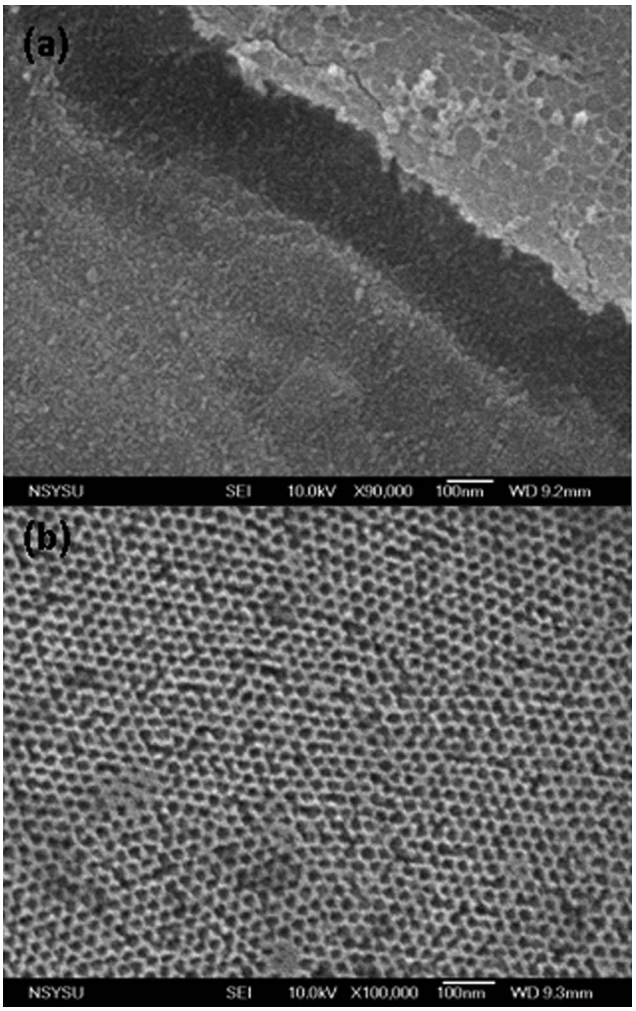

Fig. 4 FE-SEM images of mesoporous silicas templated by PEO-*b*-PCL with different TEOS/PEO-*b*-PCL weight fractions: (a)1/1 and (b)5/1.

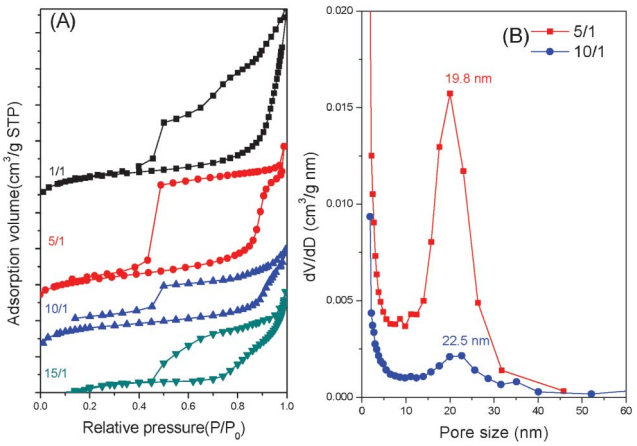

Fig. 5 (a) N_2 adsorption–desorption isotherms and (b) pore size distribution curves of mesoporous silicas templated by PEO-*b*-PCL with different TEOS/PEO-*b*-PCL weight fractions.

corresponding to the PCL blocks and the PEO blocks.[75] However, the T_gs of pure block copolymer components were not detected using the present experimental conditions. The binary pairs of phenolic/PCL[125,126] and phenolic/PEO[113] are completely miscible in all compositions in the amorphous phase due to inter-association hydrogen bonding between the hydroxyl group of phenolic and the carbonyl group of PCL and ether group of PEO, respectively; this effect has been reported in our previous studies.[113] Clearly, the two values of T_g became closer when phenolic resin contents increased, as shown in Fig. 6a. This result indicated that microphase separation (ordered structure) occurred at lower phenolic contents (<60 wt%). A single T_g corresponding to a miscible phenolic/PEO-*b*-PCL blend was comprised of up to 70 wt% phenolic resin, which is consistent with ternary phenolic/PEO/PCL blends (> 65 wt% phenolic are miscible).[64] The miscibility between these two components is due to the formation of strong intermolecular hydrogen bonding. Phenolic acts as a common solvent for PCL and PEO and induces the blends to become completely miscible (disorder structure) at higher phenolic resin contents. As shown in Fig. 6b and 6c, pure PEO-*b*-PCL displays two crystallization temperatures at 29 and 36 °C, which is also shown in Fig. 1. The two crystallization peaks became one single peak as the phenolic resin content increased (< 40 wt%). Additionally, the lowest T_f was observed at −6 °C for phenolic/PEO-*b*-PCL = 40/60, which was different than with the TEOS/PEO-*b*-PCL system. A further increase in phenolic content only showed glass transition temperatures. This result was consistent with the second heating scan in Fig. 6a that showed no melting peaks at phenolic resin contents above 50 wt%. The single exothermic peak was likely

Table 1 Textual properties of the mesoporous silicas, phenolic resins and carbon products

Sample	*d* (nm)[a]	Pore size (nm)	S_{BET} ($m^2\ g^{-1}$)[b]	S_M ($m^2\ g^{-1}$)[b]	Pore volume ($cm^3\ g^{-1}$)	Micropore volume ($cm^3\ g^{-1}$)	TEOS/PEO-*b*-PCL[c]	Morphology
Silica-*a*	23.5	—	1188	389	2.70	0.17	1/1	Long cylinder
Silica-*b*	24.1	19.8	170	50	0.33	0.02	5/1	Short cylinder
Silica-*c*	29.9	22.5	106	64	0.11	0.03	10/1	Distorted short cylinder
Silica-*d*	—	—	71	18	0.08	0.01	15/1	Disorder
							Phenolic/PEO-*b*-PCL[d]	
Phenolic-*a*	22.4	15.6	403	202	0.42	0.09	40/60	Short-range order
Phenolic-*b*	23.6	13.9	328	143	0.35	0.07	50/50	Gyroid
Phenolic-*c*	23.6	11.0	68	22	0.07	0.01	60/40	Distorted short cylinder
Phenolic-*d*	—	—	—	—	—	—	70/30	Disorder
Carbon[e]	18.6	11.0	858	647	0.59	0.30	50/50	gyroid

[a] The d-spacing values were calculated by the formula $d = 2\pi/q^*$. [b] SBET and SM are the total BET surface area and micropore surface area calculated from the *t*-plots, respectively. [c] Mesoporous silicas were prepared from 0.1 g of $EO_{114}CL_{84}$ and 0.1 g of 0.1 M $HCl_{(aq)}$. [d] Mesoporous phenolic resins were prepared from 0.1 g of $EO_{114}CL_{84}$. [e] Mesoporous carbon was synthesized from phenolic-b pyrolyzed at 800° C in N_2.

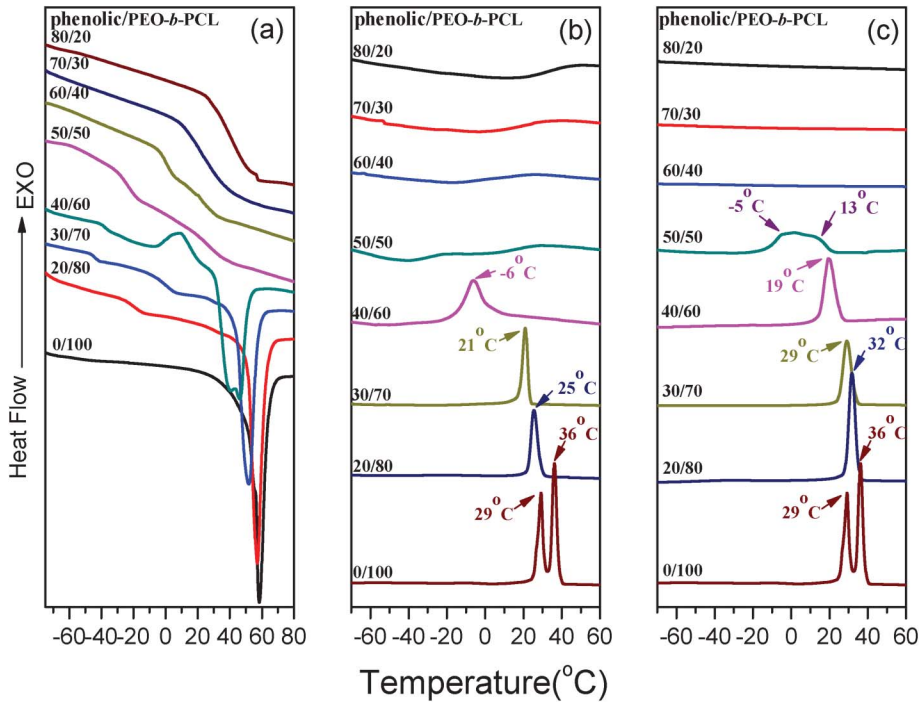

Fig. 6 DSC thermograms of (a) second heat scan and (b) first cooling scan of phenolic/PEO-*b*-PCL blends, (c) first cooling scan of phenolic/PEO-*b*-PCL blends after curing.

from the crystallization of the PCL block, because most hydroxyl groups in the phenolic resin were preferably interacting with the oxygen atoms in PEO at lower phenolic contents. The result indicated relatively lower hydrogen-bonded carbonyl groups in PCL, and the PCL phase was excluded from the phenolic/PEO phase to form a more regular microphase separation structure. The primary reason for microphase separation was due to the inter-association equilibrium constant at 264 (K_A = 264) of the hydroxyl-ether of phenolic/PEO, which was found to be substantially higher than the K_A (K_A = 116.8) from the hydroxyl-carbonyl formation of phenolic/PCL.[113]

FTIR spectroscopy is an excellent tool for detecting hydroxyl, carbonyl, and ether vibrations in blend systems. Phenolic resin shows excellent potential as a proton donor for hydrogen bonding interactions with proton-acceptor polymers because the hydroxyl group is easily accessible in the 4-position of the aromatic ring. As shown in Fig. S4a (ESI†), pure phenolic exhibits two bands in the hydroxyl-stretching region. The self-associated hydroxyl group absorption was located at 3350 cm^{-1} and was primarily due to the wide distribution of hydrogen-bonded hydroxyl groups (self-associated). The free hydroxyl groups displayed a band at 3525 cm^{-1}. As the concentration of the block copolymer increased, the intensity of the free hydroxyl band decreased and disappeared, implying the formation of hydrogen-bonding between the hydroxyl group of phenolic and PEO-ether or PCL-carbonyl groups. In addition, Fig. S7a (ESI†) displays the hydroxyl group shifting to a lower wavenumber when the PEO-*b*-PCL is the rich content in the blend (lower phenolic content), implying that the phenolic hydroxyl preferably interacts with the PEO ether. Therefore, it is reasonable to assign the band at 3250 cm^{-1} to the hydrogen-bonded hydroxyl with the ether because a relatively smaller number of the hydroxyl groups appeared to interact completely with the ether groups of the PEO block to form hydrogen-bonds. The peak frequency of the broad band shifted higher with increasing phenolic content. A new distribution of hydrogen-bonding formation resulted from the competition between the hydroxyl-hydroxyl group within the pure phenolic and the hydroxyl-carbonyl group between phenolic and PCL (3410 cm^{-1}).

The carbonyl group in the PCL blocks is also sensitive to hydrogen-bonding interactions (Fig. S4b, ESI†). The carbonyl stretching for the pure PCL is split into two bands: absorptions by the amorphous and the crystalline conformations at 1734 cm^{-1} and 1724 cm^{-1}, respectively. The crystalline conformation at 1724 cm^{-1} disappeared with an increase in phenolic content. An additional band appearing at approximately 1703 cm^{-1} was assigned as the PCL carbonyl group that was hydrogen-bonded to the phenolic hydroxyl group. The carbonyl stretching frequency split into only two bands at 1734 cm^{-1} and 1705 cm^{-1}, corresponding to the free and the hydrogen-bonded carbonyl groups, respectively. It is clear that the phenolic hydroxyl is able to form hydrogen bonds with both PEO and PCL when the phenolic content is above 40 wt% (Table S1, ESI†). The hydroxyl groups of phenolic formed hydrogen bonds only preferentially with the ether of PEO when the phenolic content was below 40 wt%, indicating the PCL phase was excluded from the phenolic/PEO phase (relative lower fraction of H-bonded C=O group of PCL); this result was consistent with DSC analyses.

The structures of mesoporous phenolic resins that were templated by the double crystalline amphiphilic diblock copolymer PEO-*b*-PCL were also investigated using TEM and SAXS, as shown in Fig. 7 and 8. These figures suggest that the phenolic contents have an influence on the formation of the

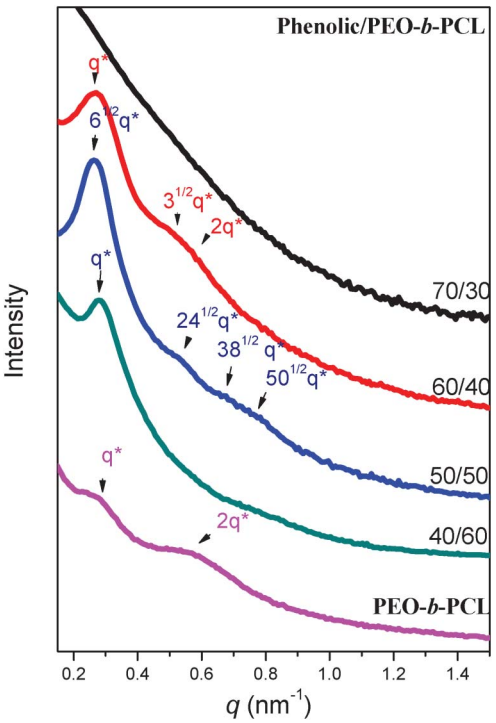

Fig. 7 SAXS patterns of mesoporous phenolic resins from different weight fractions of phenolic/PEO-*b*-PCL blends.

mesostructure. In SAXS, pure PEO-*b*-PCL block copolymer revealed a lamellae character for the special ratio of q^* and $2q^*$. A remarkable mesophase transformation through short range order, gyroid, short cylinder and finally to disordered structures was observed with an increase in phenolic resin contents. The short-range order morphology was observed when phenolic/PEO-*b*-PCL = 40/60 (phenolic-*a*) by SAXS analysis, as shown in Fig. 7a. Based on only one scattering peak at $q^* = 0.27$ nm^{-1}, $d = 23.2$ nm was consistent with the TEM image in Fig. 8a. There was not enough phenolic resin to include the template PEO-*b*-PCL block copolymer and to form a complete mesoporous structure. A highly-ordered bicontinuous gyroid structure was observed at phenolic/PEO-*b*-PCL = 50/50 (phenolic-*b*) based on SAXS and TEM. In SAXS patterns, as shown in Fig. 7b, the intensity maximum appears at $6^{1/2}q^* = 0.26$ nm^{-1} ($d = 24.1$ nm). The higher-order reflections at $24^{1/2}q^*$, $38^{1/2}q^*$ and $50^{1/2}q^*$ were observed, which are characteristic for a long-range order of bicontinuous gyroid structure, and were further confirmed by TEM images, as shown in Fig. 8b. When phenolic/PEO-*b*-PCL = 40/60 (phenolic-*c*), the maximum intensity appeared at approximately $q^* = 0.26$ nm^{-1} ($d = 24.1$ nm) and had a higher-order reflection at $3^{1/2}q^*$ and $2q^*$, as seen in Fig. 7c. These values were characteristic for a short cylindrical structure, which was further confirmed by TEM due to the volume fraction of phenolic resin raising the outer domain as shown in Fig. 8c. However, it presented a disordered structure when the ratio increased to phenolic/PEO-*b*-PCL = 70/30 (phenolic-*d*), by the SAXS analysis in Fig. 7d. This analysis presented broad peaks that indicated the absence of a long-range ordered structure, which was further confirmed in Fig. 8d by TEM. This result also agreed with DSC and FTIR analyses. The phenolic hydroxyl was able to form hydrogen bonds with both PEO and PCL according to FTIR spectroscopy (Fig. S4, ESI†). A completely miscible blend by

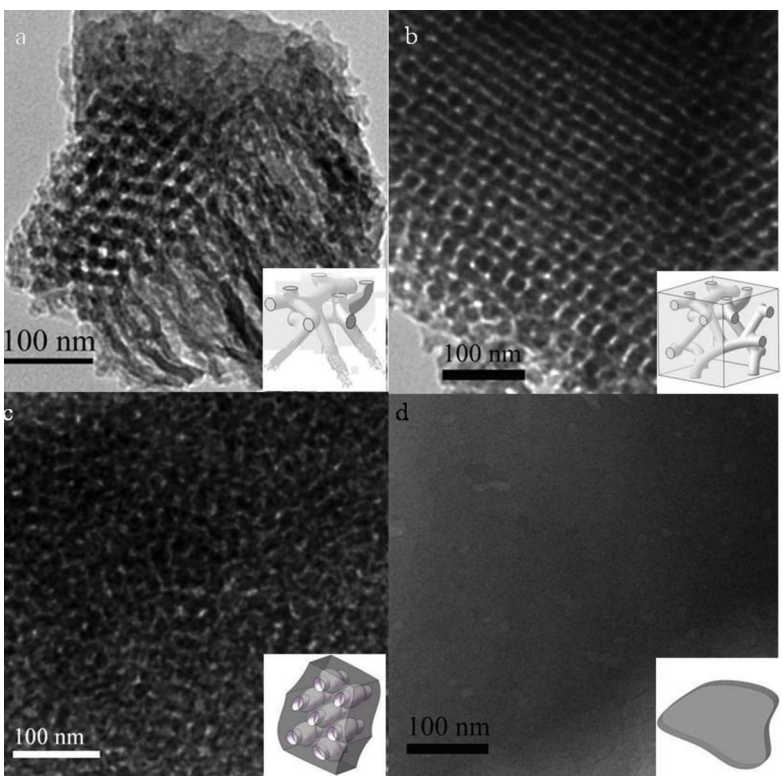

Fig. 8 TEM image of mesoporous phenolic resins from different weight fractions of phenolic/PEO-*b*-PCL blends: (a) 40/60, (b) 50/50, (c) 60/40, and (d) 70/30.

DSC analysis was due to only one single T_g in Fig. 6 when the phenolic content was at 70 wt%.

Mesoporous phenolic resins exhibited similar N_2 sorption isotherms to mesoporous silicas, as shown in Fig. 9A. N_2 sorption isotherms of mesoporous phenolic resins behaved like representative type IV curves with a sharp capillary condensation step in the relative pressure range of 0.85 to 0.95. These data indicated the generation of mesopores with a large uniform size. The phenolic-*a* and phenolic-*b* samples exhibited a typical H_1-like hysteresis loop at P/P_0 = 0.4 to 0.9, indicating a common mesoporous structure with branched cylindrical large pores. The H_1 hysteresis loop found for phenolic-*a* was the characteristic of the cylindrical mesopores. Based on the Harkins and Jura model, the mean pore size measured from the adsorption branch was as large as 15.6 nm, as shown in Fig. 9B. Similar isotherms with the H_1-type hysteresis loops could also be detected for phenolic-*b*. The mean pore size (Fig. 9B) of phenolic-*b* calculated from the Harkins and Jura model (13.9 nm) was similar, but slightly smaller, than that of phenolic-*a*. The total pore volume and the total BET surface area of phenolic-*b* were 0.35 $cm^3\ g^{-1}$ and 328 $m^2\ g^{-1}$, respectively. These values were much larger than that of phenolic-*c* (Table 1), confirming the presence of the distorted short cylinder mesopores that were transferred from the cylindrical mesopores of the gyroid structure. To the best of our knowledge, this study is the first to fabricate a long-range order of bicontinuous gyroid type mesoporous phenolic resin using an EISA strategy. The BET surface area, pore volume and BJH pore size of mesoporous phenolic resins are summarized in Table 1.

Furthermore, a special appearance was found in the SAXS of the mesoporous silicas and phenolic resins with an increase in the ratio of TEOS/PEO-*b*-PCL or phenolic/PEO-*b*-PCL as shown in Scheme 2. The *d*-spacing of the mesoporous silicas and phenolic resins showed a similar phenomenon that both increased upon increasing the ratios of TEOS/PEO-*b*-PCL and phenolic/PEO-*b*-PCL. However, the pore size of mesoporous silicas increased when increasing the ratio of TEOS/PEO-*b*-PCL. The mesoporous phenolic resins presented different trends that became smaller when increasing the ratio of phenolic/PEO-*b*-PCL, as shown in Table 1. This result is described by the different intermolecular hydrogen-bonding interactions between silica precursors or uncured phenolic resin with the PEO-*b*-PCL block copolymer. It was expected that the intermolecular hydrogen bonding strength of phenolic–OH with PEO was stronger than that of Si–OH with PEO.[127,128] As a result, the uncured phenolic resin would dissolve in both PEO and PCL blocks, but silica precursors would only locate at the corona of micelle in the PEO-*b*-PCL diblock copolymers. In addition, the hydroxyl group of the phenolic resin will also interact with the carbonyl of the PCL block at relative higher phenolic contents, resulting in the decrease of mesopore size after calcinations. This interaction will not occur in the silica system. Fig. S5 (ESI†) shows photograph images of a cured phenolic/PEO-*b*-PCL = 50/50 blend and its pyrolyzed product, implying that we can maintain the original shape of phenolic/PEO-*b*-PCL thin film after calcinations. The mesoporous phenolic resin thin film can be obtained and applied to various fields such as mesoporous carbon (Fig. S6 and S7, ESI†).

Conclusions

We have successfully synthesized crystalline–crystalline block copolymers of PEO-*b*-PCL in the present study. DSC, FTIR,

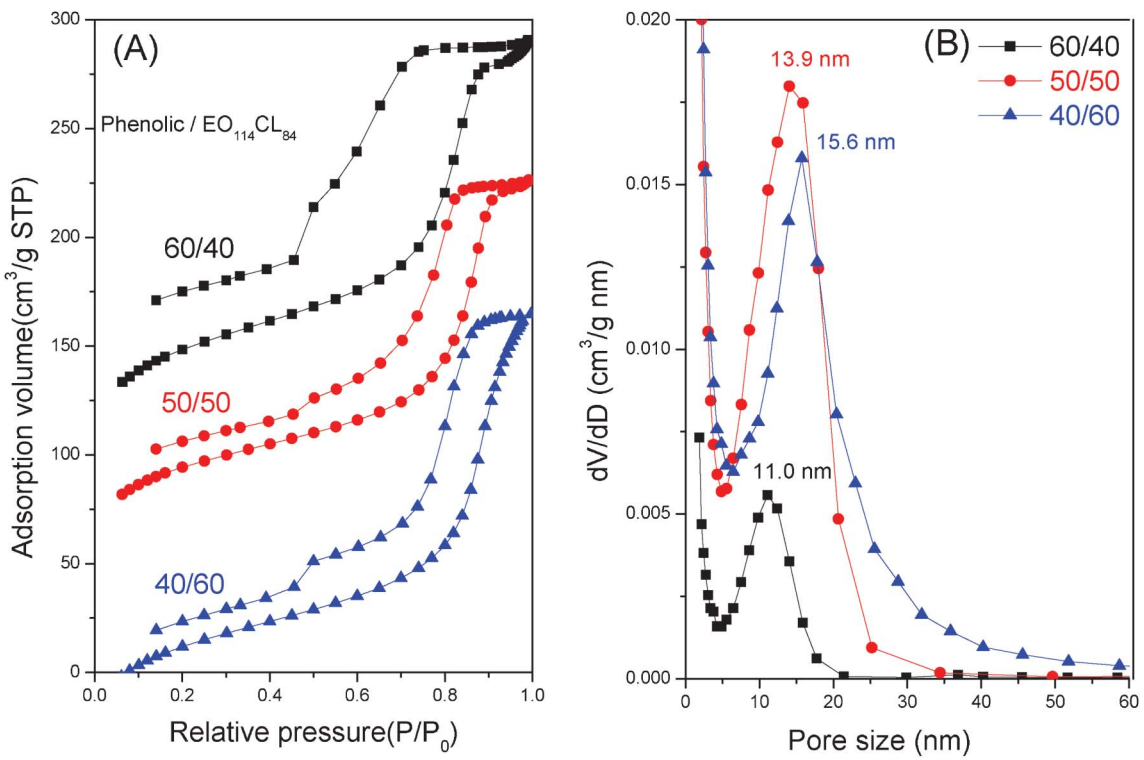

Fig. 9 (A) N_2 adsorption–desorption isotherms and (B) pore size distribution curves of mesoporous resins templated by PEO-*b*-PCL with different phenolic/PEO-*b*-PCL weight fractions.

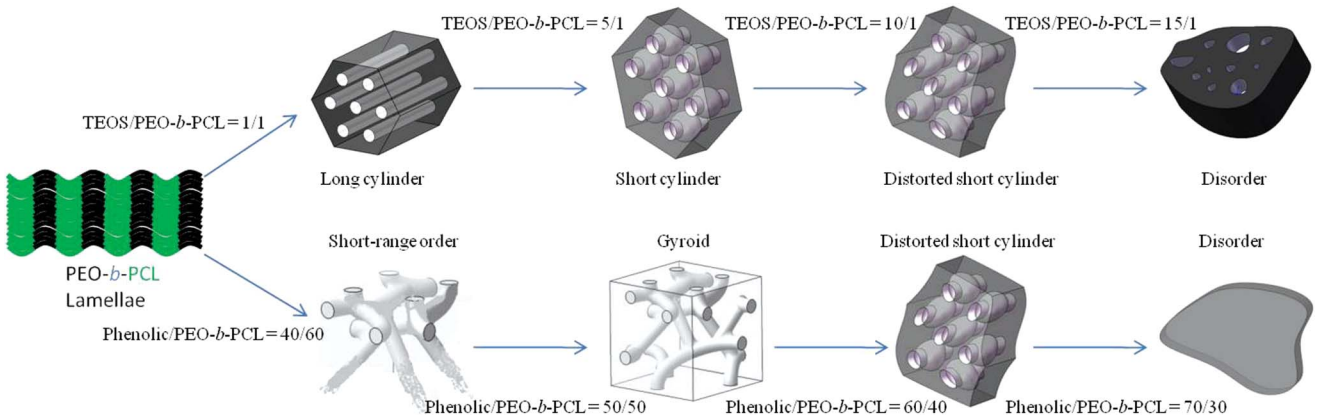

Scheme 2 Morphology changes in mesoporous silicas and mesoporous phenolic resin.

SAXS and TEM techniques were employed to investigate the crystalline behavior, competing hydrogen bonding interaction and mesoporous nanostructure of silicas and phenolic resins. The cooling results from DSC showed that the structure transition of PCL occurred through the T_f of PCL changing. TEM images and SAXS analyses indicated that different compositions of TEOS/PEO-*b*-PCL or phenolic/PEO-*b*-PCL blends resulted in different mesoporous nanostructures through the mediation of hydrogen bonding interactions between silica, phenolic resins and the PEO-*b*-PCL block copolymer. FT-IR spectra also provided evidence that the PEO ether group was a stronger hydrogen bond acceptor than the PCL carbonyl group. We obtained different mesoporous nanostructures of silicas and phenolic resins.

Acknowledgements

This work was supported financially by the National Science Council, Taiwan, Republic of China, under Contract No. NSC 97-2221-E-110-013-MY3 and NSC-99-2628-E-110-003.

References

1 X. Zhuang, Y. Wan, C. M. Feng, Y. Shen and D. Y. Zhao, *Chem. Mater.*, 2009, **21**, 706.
2 Z. X. Wu, Y. X. Yang, B. Tu, P. A. Webley and D. Y. Zhao, Adsorpt.-J. Int. *Adsorpt. Soc.*, 2009, **15**, 123.
3 S. B. Wang, *Microporous Mesoporous Mater.*, 2009, **117**, 1.
4 G. Oye, W. R. Glomm, T. Vralstad, S. Volden, H. Magnusson, M. Stocker and J. Sjoblom, *Adv. Colloid Interface Sci.*, 2006, **123**, 17.
5 M. Hartmann, A. Vinu and G. Chandrasekar, *Chem. Mater.*, 2005, **17**, 829.
6 M. Hartmann, *Chem. Mater.*, 2005, **17**, 4577.
7 C. Z. Yu, J. Fan, B. Z. Tian and D. Y. Zhao, *Chem. Mater.*, 2004, **16**, 889.
8 A. Vinu, V. Murugesan, O. Tangermann and M. Hartmann, *Chem. Mater.*, 2004, **16**, 3056.
9 A. Sayari and S. Hamoudi, *Chem. Mater.*, 2001, **13**, 3151.
10 Z. X. Wu, Y. Meng and D. Y. Zhao, *Microporous Mesoporous Mater.*, 2010, **128**, 1.
11 K. Nakajima, T. Fukui, H. Kato, M. Kitano, J. N. Kondo, S. Hayashi and M. Hara, *Chem. Mater.*, 2010, **22**, 3332.
12 H. A. Meng, M. Liong, T. A. Xia, Z. X. Li, Z. X. Ji, J. I. Zink and A. E. Nel, *ACS Nano*, 2010, **4**, 4539.
13 R. M. Martin-Aranda and J. Cejka, *Top. Catal.*, 2010, **53**, 141.
14 N. Hao, Y. X. Yang, H. T. Wang, P. A. Webley and D. Y. Zhao, *J. Colloid Interface Sci.*, 2010, **346**, 429.
15 F. Chen, X. J. Meng and F. S. Xiao, *Catal. Surv. Asia*, 2011, **15**, 37.
16 J. Cejka and S. Mintova, *Catal. Rev. Sci. Eng.*, 2007, **49**, 457.
17 L. H. Chen, G. S. Zhu, D. L. Zhang, H. Zhao, M. Y. Guo, S. B. Wei and S. L. Qiu, *J. Mater. Chem.*, 2009, **19**, 2013.
18 Y. Chen, H. R. Chen, M. Ma, F. Chen, L. M. Guo, L. X. Zhang and J. L. Shi, *J. Mater. Chem.*, 2011, **21**, 5290.
19 T. L. Chew, A. L. Ahmad and S. Bhatia, *Adv. Colloid Interface Sci.*, 2010, **153**, 43.
20 N. Ehlert, M. Badar, A. Christel, S. J. Lohmeier, T. Luessenhop, M. Stieve, T. Lenarz, P. P. Mueller and P. Behrens, *J. Mater. Chem.*, 2011, **21**, 752.
21 Q. Gao, W. J. Xu, Y. Xu, D. Wu, Y. H. Sun, F. Deng and W. L. Shen, *J. Phys. Chem. B*, 2008, **112**, 2261–2267.
22 Q. J. He and J. L. Shi, *J. Mater. Chem.*, 2011, **21**, 5845.
23 T. Heikkila, J. Salonen, J. Tuura, M. S. Hamdy, G. Mul, N. Kumar, T. Salmi, D. Y. Murzin, L. Laitinen, A. M. Kaukonen, J. Hirvonen and V. P. Lehto, *Int. J. Pharm.*, 2007, **331**, 133.
24 T. Heikkila, J. Salonen, J. Tuura, N. Kumar, T. Salmi, D. Y. Murzin, M. S. Hamdy, G. Mul, L. Laitinen, A. M. Kaukonen, J. Hirvonen and V. P. Lehto, *Drug Delivery*, 2007, **14**, 337.
25 G. M. Liu, S. R. Zheng, D. Q. Yin, Z. Y. Xu, J. Fan and F. Jiang, *J. Colloid Interface Sci.*, 2006, **302**, 47.
26 B. V. Lotsch and G. A. Ozin, *ACS Nano*, 2008, **2**, 2065.
27 M. M. Mekawy, A. Yamaguchi, S. A. El-Safty, T. Itoh and N. Teramae, *J. Colloid Interface Sci.*, 2011, **355**, 348.
28 H. A. Meng, M. Liong, T. A. Xia, Z. X. Li, Z. X. Ji, J. I. Zink and A. E. Nel, *ACS Nano*, 2010, **4**, 4539.
29 G. J. Parker, M. D. B. Charlton, M. E. Zoorob, J. J. Baumberg, M. C. Netti and T. Lee, *Philos. Trans. R. Soc. London, Ser. A*, 2006, **364**, 189.
30 L. Peng, A. Philippaerts, X. X. Ke, J. Van Noyen, F. De Clippel, G. Van Tendeloo, P. A. Jacobs and B. F. Sels, *Catal. Today*, 2010, **150**, 140.
31 J. Salonen, A. M. Kaukonen, J. Hirvonen and V. P. Lehto, *J. Pharm. Sci.*, 2008, **97**, 632.
32 S. Shylesh, P. P. Samuel, S. Sisodiya and A. P. Singh, *Catal. Surv. Asia*, 2008, **12**, 266.
33 A. Vinu, K. Z. Hossian, P. Srinivasu, M. Miyahara, S. Anandan, N. Gokulakrishnan, T. Mori, K. Ariga and V. V. Balasubramanian, *J. Mater. Chem.*, 2007, **17**, 1819.
34 A. Vinu, M. Miyahara and K. Ariga, *J. Nanosci. Nanotechnol.*, 2006, **6**, 1510.
35 A. Vinu, M. Miyahara, V. Sivamurugan, T. Mori and K. Ariga, *J. Mater. Chem.*, 2005, **15**, 5122.
36 W. Xia, J. Chang, J. P. Lin and J. Q. Zhu, *Eur. J. Pharm. Biopharm.*, 2008, **69**, 546.
37 X. C. Xu, C. S. Song, J. M. Andresen, B. G. Miller and A. W. Scaroni, *Microporous Mesoporous Mater.*, 2003, **62**, 29.
38 Q. H. Yang, J. Liu, L. Zhang and C. Li, *J. Mater. Chem.*, 2009, **19**, 1945.
39 X. Yuan, W. Xing, S. P. Zhuo, W. J. Si, X. L. Gao, Z. H. Han and Z. F. Yan, *J. Colloid Interface Sci.*, 2008, **322**, 558.
40 Z. Y. Yuan and B. L. Su, *J. Mater. Chem.*, 2006, **16**, 663.
41 M. Zhang, Y. P. Wu, X. Z. Feng, X. W. He, L. X. Chen and Y. K. Zhang, *J. Mater. Chem.*, 2010, **20**, 5835.

42 Y. X. Zhang, S. C. Xu, Y. Y. Luo, S. S. Pan, H. L. Ding and G. H. Li, *J. Mater. Chem.*, 2011, **21**, 3664.
43 W. R. Zhao, M. D. Lang, Y. S. Li, L. Li and J. L. Shi, *J. Mater. Chem.*, 2009, **19**, 2778.
44 C. L. Zhu, X. Y. Song, W. H. Zhou, H. H. Yang, Y. H. Wen and X. R. Wang, *J. Mater. Chem.*, 2009, **19**, 7765.
45 J. S. Beck, J. C. Vartuli, W. J. Roth, M. E. Leonowicz, C. T. Kresge, K. D. Schmitt, C. T. W. Chu, D. H. Olson, E. W. Sheppard, S. B. McCullen, J. B. Higgins and J. L. Schlenker, *J. Am. Chem. Soc.*, 1992, **114**, 10834.
46 C. T. Kresge, M. E. Leonowicz, W. J. Roth, J. C. Vartuli and J. S. Beck, *Nature*, 1992, **359**, 710.
47 A. Corma, *Chem. Rev.*, 1997, **97**, 2373.
48 Q. S. Huo, D. I. Margolese and G. D. Stucky, *Chem. Mater.*, 1996, **8**, 1147.
49 J. C. Vartuli, K. D. Schmitt, C. T. Kresge, W. J. Roth, M. E. Leonowicz, S. B. McCullen, S. D. Hellring, J. S. Beck, J. L. Schlenker, D. H. Olson and E. W. Sheppard, *Chem. Mater.*, 1994, **6**, 2317.
50 H. Yang, N. Coombs and G. A. Ozin, *Nature*, 1997, **386**, 692.
51 J. M. Seddon and M. E. Raimondi, *Mol. Cryst. Liq. Cryst.*, 2000, **347**, 465.
52 C. Z. Yu, J. Fan, B. Z. Tian and D. Y. Zhao, *Chem. Mater.*, 2004, **16**, 889.
53 C. J. Brinker, Y. F. Lu, A. Sellinger and H. Y. Fan, *Adv . Mater.*, 1999, 11.
54 Y. Deng, C. Liu, D. Gu, T. Yu, B. Tu and D. Y. Zhao, *J. Mater. Chem.*, 2008, **18**, 91.
55 Y. H. Deng, T. Yu, Y. Wan, Y. F. Shi, Y. Meng, D. Gu, L. J. Zhang, Y. Huang, C. Liu, X. J. Wu and D. Y. Zhao, *J. Am. Chem. Soc.*, 2007, **129**, 1690.
56 D. Grosso, C. Boissiere, B. Smarsly, T. Brezesinski, N. Pinna, P. A. Albouy, H. Amenitsch, M. Antonietti and C. Sanchez, *Nat. Mater.*, 2004, **3**, 787.
57 Y. Huang, J. P. Yang, H. Q. Cai, Y. P. Zhai, D. Feng, Y. H. Deng, B. Tu and D. Y. Zhao, *J. Mater. Chem.*, 2009, **19**, 6536.
58 Y. Meng, D. Gu, F. Q. Zhang, Y. F. Shi, L. Cheng, D. Feng, Z. X. Wu, Z. X. Chen, Y. Wan, A. Stein and D. Y. Zhao, *Chem. Mater.*, 2006, **18**, 4447.
59 S. Valkama, A. Nykanen, H. Kosonen, R. Ramani, F. Tuomisto, P. Engelhardt, G. ten Brinke, O. Ikkala and J. Ruokolainen, *Adv. Funct. Mater.*, 2007, **17**, 183.
60 Y. Wan, Y. F. Shi and D. Y. Zhao, *Chem. Commun.*, 2007, 897.
61 K. Yu, A. J. Hurd, A. Eisenberg and C. J. Brinker, *Langmuir*, 2001, **17**, 7961.
62 K. Kailasam, Y. S. Jun, P. Katekomol, J. D. Epping, W. H. Hong and A. Thomas, *Chem. Mater.*, 2010, **22**, 428.
63 J. Y. Zhang, Y. H. Deng, J. Wei, Z. K. Sun, D. Gu, H. Bongard, C. Liu, H. H. Wu, B. Tu, F. Schuth and D. Y. Zhao, *Chem. Mater.*, 2009, **21**, 3996.
64 R. L. Liu, Y. F. Shi, Y. Wan, Y. Meng, F. Q. Zhang, D. Gu, Z. X. Chen, B. Tu and D. Y. Zhao, *J. Am. Chem. Soc.*, 2006, **128**, 11652.
65 C. Liu, Y. H. Deng, J. Liu, H. H. Wu and D. Y. Zhao, *Microporous Mesoporous Mater.*, 2008, **116**, 633.
66 J. Rodriguez-Hernandez, F. Checot, Y. Gnanou and S. Lecommandoux, *Prog. Polym. Sci.*, 2005, **30**, 691.
67 I. U. Hamley, *The Physics of Block Copolymers*; Oxford University Press: Oxford, UK, 1998.
68 S. Foerster and M. Antonietti, *Adv. Mater.*, 1998, **10**, 195.
69 N. Hadjichristidis, S. Pispas and G. A. Floudas, *Block Copolymers Synthetic Strategies, Physical Properties, and Applications*; John Wiley& Sons: Hoboken, 2003.
70 W. C. Chen, S. W. Kuo, U. S. Jeng and F. C. Chang, *Macromolecules*, 2008, **41**, 1401.
71 W. C. Chen, S. W. Kuo, C. H. Lu, U. S. Jeng and F. C. Chang, *Macromolecules*, 2009, **42**, 3580.
72 N. Hameed and Q. P. Guo, *Polymer*, 2008, **49**, 922.
73 N. Hameed, N. V. Salim and Q. P. Guo, *J. Chem. Phys.*, 2009, **131**, 214905.
74 I. H. Lin, S. W. Kuo and F. C. Chang, *Polymer*, 2009, **50**, 5276.
75 N. V. Salim, T. Hanley and Q. P. Guo, *Macromolecules*, 2010, **43**, 7695.
76 D. Y. Zhao, J. L. Feng, Q. S. Huo, N. Melosh, G. H. Fredrickson, B. F. Chmelka and G. D. Stucky, *Science*, 1998, **279**, 548.
77 D. Y. Zhao, Q. S. Huo, J. L. Feng, B. F. Chmelka and G. D. Stucky, *J. Am. Chem. Soc.*, 1998, **120**, 6024.
78 X. Y. Bao, X. S. Zhao, X. Li, P. A. Chia and J. Li, *J. Phys. Chem. B*, 2004, **108**, 4684.
79 L. Cao and M. Kruk, *Colloids Surf., A*, 2010, **357**, 91.
80 J. P. Hanrahan, A. Donovan, M. A. Morris and J. D. Holmes, *J. Mater. Chem.*, 2007, **17**, 3881.
81 S. S. Kim, A. Karkamkar, T. J. Pinnavaia, M. Kruk and M. Jaroniec, *J. Phys. Chem. B*, 2001, **105**, 7663.
82 T. W. Kim, F. Kleitz, B. Paul and R. Ryoo, *J. Am. Chem. Soc.*, 2005, **127**, 7601.
83 B. Z. Tian, X. Y. Liu, Z. D. Zhang, B. Tu and D. Y. Zhao, *J. Solid State Chem*, 2002, **167**, 324.
84 D. H. Chen, Z. W. Li, Y. X. J. Tu, Y. F. Shi, Z. X. Chen, W. Shen, C. Z. Yu, B. Tu and D. Y. Zhao, *J. Mater. Chem.*, 2006, **16**, 1511.
85 J. Lee, J. Kim, Y. Lee, S. Yoon, S. M. Oh and T. Hyeon, *Chem. Mater.*, 2004, **16**, 3323.
86 Z. Y. Wang and A. Stein, *Chem. Mater.*, 2008, **20**, 1029.
87 F. Q. Zhang, Y. Meng, D. Gu, Y. Yan, Z. X. Chen, B. Tu and D. Y. Zhao, *Chem. Mater.*, 2006, **18**, 5279.
88 J. Tang, Y. B. Fan, J. Hu and H. L. Liu, *J. Colloid Interface Sci.*, 2009, **331**, 191.
89 L. Y. Song, D. Feng, C. G. Campbell, D. Gu, A. M. Forster, K. G. Yager, N. Fredin, H. J. Lee, R. L. Jones, D. Y. Zhao and B. D. Vogt, *J. Mater. Chem.*, 2010, **20**, 1691.
90 C. Urata, Y. Tamura, Y. Yamauchi and K. Kuroda, *J. Mater. Chem.*, 2011, **21**, 3711.
91 G. W. Zhou, Y. J. Chen, J. H. Yang and S. H. Yang, *J. Mater. Chem.*, 2007, **17**, 2839.
92 H. P. Lin, C. Y. Chang-Chien, C. Y. Tang and C. Y. Lin, *Microporous Mesoporous Mater.*, 2006, **93**, 344.
93 M. H. Sorensen, R. W. Corkery, J. S. Pedersen, J. Rosenholm and P. C. Alberius, *Microporous Mesoporous Mater.*, 2008, **113**, 1.
94 L. M. Wang, B. Z. Tian, J. Fan, X. Y. Liu, H. F. Yang, C. Z. Yu, B. Tu and D. Y. Zhao, *Microporous Mesoporous Mater.*, 2004, **67**, 123.
95 J. F. Yao, H. T. Wang, K. Y. Chan, L. X. Zhang and N. P. Xu, *Microporous Mesoporous Mater.*, 2005, **82**, 183.
96 F. Q. Zhang, Y. Yan, Y. Meng, Y. Xia, B. Tu and D. Y. Zhao, *Microporous Mesoporous Mater.*, 2007, **98**, 6.
97 A. Soininen, S. Valkama, A. Nykanen, A. Laiho, H. Kosonen and R. Mezzenga, *Chem. Mater.*, 2007, **19**, 3093.
98 Y. Wan, Y. F. Shi and D. Y. Zhao, *Chem. Mater.*, 2008, **20**, 932.
99 Y. Meng, D. Gu, F. Q. Zhang, Y. F. Shi, H. F. Yang, Z. Li, C. Z. Yu, B. Tu and D. Y. Zhao, *Angew. Chem., Int. Ed.*, 2005, **44**, 7053.
100 J. Jin, N. Nishiyama, Y. Egashira and K. Ueyama, *Microporous Mesoporous Mater.*, 2009, **118**, 218.
101 X. F. Qian, H. X. Li and Y. Wan, *Microporous Mesoporous Mater.*, 2011, **141**, 26.
102 B. D. Vogt, V. L. Chavez, M. Z. Dai, M. R. C. Arreola, L. Y. Song, D. Feng, D. Y. Zhao, G. M. Perera and G. E. Stein, *Langmuir*, 2011, **27**, 5607.
103 C. F. Xue, B. Tu and D. Y. Zhao, *Nano Res.*, 2009, **2**, 242.
104 F. Q. Zhang, D. Gu, T. Yu, F. Zhang, S. H. Xie, L. J. Zhang, Y. H. Deng, Y. Wan, B. Tu and D. Y. Zhao, *J. Am. Chem. Soc.*, 2007, **129**, 7746.
105 F. Kleitz, S. H. Choi and R. Ryoo, *Chem. Commun.*, 2003, 2136.
106 H. F. Yang and D. Y. Zhao, *J. Mater. Chem*, 2005, **15**, 1217.
107 K. P. Gierszal, T. W. Kim, R. Ryoo and M. Jaroniec, *J. Phys. Chem. B*, 2005, **109**, 23263.
108 R. Ryoo, S. H. Joo, M. Kruk and M. Jaroniec, *Adv. Mater.*, 2001, **13**, 677.
109 H. F. Lee, S. W. Kuo, C. F. Huang, J. S. Lu, S. C. Chan, C. F. Wang and F. C. Chang, *Macromolecules*, 2006, **39**, 5458.
110 S. C. Chen, S. W. Kuo, U. S. Jeng and F. C. Chang, *Macromolecules*, 2010, **43**, 1083.
111 C. H. Lu, S. W. Kuo and F. C. Chang, *Macromol. Rapid Commun.*, 2009, **30**, 2121.
112 W. C. Chen, S. W. Kuo and F. C. Chang, *Polymer*, 2010, **51**, 4176.
113 S. W. Kuo, C. L. Lin and F. C. Chang, *Macromolecules*, 2002, **35**, 278.
114 H. L. Chen, S. C. Hsiao, T. L. Lin, K. Yamauchi, H. Hasegawa and T. Hashimoto, *Macromolecules*, 2001, **34**, 671.
115 H. C. Lin, S. W. Kuo, C. F. Huang and F. C. Chang, *Macromol. Rapid Commun.*, 2006, **27**, 537.

116 M. W. Huang, S. W. Kuo, H. D. Wu, F. C. Chang and S. Y. Fang, *Polymer*, 2002, **43**, 2479.
117 S. W. Kuo, S. C. Chan, H. D. Wu and F. C. Chang, *Macromolecules*, 2005, **38**, 4729.
118 C. F. Huang, S. W. Kuo, F. J. Lin, W. J. Huang, C. F. Wang, W. Y. Chen and F. C. Chang, *Macromolecules*, 2006, **39**, 300.
119 C. Y. Chiu, W. H. Hsu, Y. J. Yen, S. W. Kuo and F. C. Chang, *Macromolecules*, 2005, **38**, 6640.
120 H. L. Chen, J. C. Wu, T. L. Lin and J. S. Lin, *Macromolecules*, 2001, **34**, 6936.
121 Y. L. Loo, R. A. Register, A. J. Ryan and G. T. Dee, *Macromolecules*, 2001, **34**, 8968.
122 H. L. Chen, S. Y. Lin, Y. Y. Huang, F. C. Chiu, W. Liou and J. S. Lin, *Macromolecules*, 2002, **35**, 9434.
123 J. T. Xu, S. C. Turners, J. P. A. Fairclough, S. M. Mai, A. J. Ryan, C. Chaibundit and C. Booth, *Macromolecules*, 2002, **35**, 3614.
124 J. Y. Hsu, I. F. Hsieh, B. Nandan, F. C. Chiu, J. H. Chen, U. S. Jeng and H. L. Chen, *Macromolecules*, 2007, **40**, 5014.
125 S. W. Kuo and F. C. Chang, *Macromol. Chem. Phys.*, 2001, **202**, 3112.
126 S. W. Kuo, S. C. Chan and F. C. Chang, *J. Polym. Sci., Part B: Polym. Phys.*, 2004, **42**, 117.
127 M. M. Coleman, J. F. Graf and P. C. Painter, *Specific Interactions and the Miscibility of Polymer Blends*; Technomic Publishing, Lancaster, PA, 1991.
128 M. M. Coleman and P. C. Painter, *Miscible Polymer Blend-Background and Guide for Calculations and Design*; DEStech Publications, Inc, 2006.